Development and Characterization of Novel Modified Red Mud Nanocomposites Based on Poly(hydroxy ether) of Bisphenol A

A. H. Bhat,[1] H. P. S. Abdul Khalil,[1] Irshad-ul-Haq Bhat,[1] A. K. Banthia[2]

[1]*School of Industrial Technology, Universiti Sains Malaysia, Penang 11800, Malaysia*
[2]*Materials Science Centre, Indian Institute of Technology, Kharagpur 721302, India*

Received 23 July 2009; accepted 15 April 2010
DOI 10.1002/app.32654
Published online 27 July 2010 in Wiley Online Library (wileyonlinelibrary.com).

ABSTRACT: This study dealt with the use of various quantities of modified red mud as a nanofiller in a poly(hydroxy ether) of bisphenol A (Phe) based matrix. Phe-based polymer nanocomposites reinforced with acidically and organically modified layered red mud were prepared by a conventional solvent-casting technique. The best dispersion occurred in the polymer nanocomposites where the interactions between the functional groups of the polymer matrix and those of the organic substitution of the red mud appeared to be the highest. The particle size of the modified red mud was determined by field emission scanning electron microscopy. The as-synthesized composite films were typically characterized by Fourier transform infrared spectroscopy and X-ray diffraction. The dispersion of the modified fillers within the matrix was studied by transmission electron microscopy. The thermal properties measured by thermogravimetric analysis showed enhanced thermal stability of a series of composite materials. © 2010 Wiley Periodicals, Inc. J Appl Polym Sci 119: 515–522, 2011

Key words: plastics; polyethers; TEM; thermal properties; X-ray

INTRODUCTION

Filled polymer systems have gained popularity in the composite industry for both their cost and performance objectives. The use of layered inorganic fillers has been a common practice in the plastics industry to improve the properties of thermoplastics. Polymers are generally known to be good matrix materials because of their stable chemical properties. Thus, both the mechanical and thermal properties of polymers can be further improved by the addition of inorganic fillers. The effects of a filler on the material properties of composite materials depend strongly on its particle size, shape, aggregate size, surface characteristics, and degree of dispersion. Polymer composites prepared in combination with an organic component as a matrix and an inorganic component as a filler on the nanoscale[1–4] have additional advantages, such as the possibility of obtaining a material that has the advantages of both organic materials (e.g., light weight, flexibility, good moldability) and inorganic materials (e.g., high strength, heat stability, and chemical resistance).[5]

Red mud is the waste generated during aluminum production from bauxite.[6–8] It is reported that the production of 1 ton of metallic aluminum generates about 2 tons of red mud.[8] At all of the world's 85 alumina plants, 1.0–1.6 tons of red mud is generated per ton of alumina, and it is estimated that over 66 million tons of this waste is impounded annually in the world. The disposal of such a large quantity of this alkaline waste sludge is expensive (up to 1–2% of the alumina price), as it requires a lot of land (ca. 1 km^2/5 years for a 1-metric tones per year (mtpy) alumina plant) and causes a number of environmental problems.[9]

The enormous quantity of red mud generated every year poses a very serious and alarming environmental problem.[10] To solve this disposal problem, voluminous research and development work for the utilization of red mud has been carried out all over the world, but to date, very few techno-economical solutions have been discovered.[6–8,10] So far, the various uses of red mud developed include use as acidic amenders[8] and in making building materials, namely, bricks,[11] ceramics, tiles,[12] glazes,[13] red mud/polymer composites panels as wood substitutes,[14] and iron rich cement.[15] Fundamental studies carried out for the extraction of iron oxide or titanium oxide are reported to be economically unsustainable,[16] and therefore, red mud as such has been used for various applications. Red mud has also been used for the catalytic hydrodechlorination of tetrachloroethylene,[17] for the treatment of gold ores,[18] and in making silicate-bonded unsintered ceramics,[19] heavy clay products,[20] and sintered ceramics.[21]

Correspondence to: A. H. Bhat (aamir_bhat@rediffmail.com).

Recently, a new thermoplastic matrix, poly(hydroxy ether) of bisphenol A (Phe),[22] was reported to be able to significantly disperse a commercial organically modified montmorillonite: Cloisite20A. The mechanical properties, such as the modulus of elasticity and the yield stress, showed significant improvement, with values comparable to the largest obtained with other polymer matrices. Nanoscale fillers differ from bulk materials and conventional micrometer-size fillers because of their small size and corresponding increase in the aspect ratio.

There have been publications associated with the preparation and characterization of poly(vinyl alcohol)-modified red mud composite materials.[23] The improvement of red mud polymer/matrix composites by the organophilization of red mud has also been studied with poly(vinyl alcohol) as the matrix material.[24] Chand and Hashmi[25,26] tried to improve the mechanical properties and abrasive wear properties of polymer blends filled with red mud.

The challenges in this area of high-performance organic–inorganic hybrid materials are to obtain significant improvements in the interfacial adhesion between the polymer matrix and the reinforcing material because the organic matrix is relatively incompatible with the inorganic phase. Generally, better interfacial bonding will impart better properties, such as high modulus, strength, and stiffness, to a polymer composite.[6–7]

The aim of this study was to examine the effect of chemical surface treatments of red mud with inorganic acids and organic moieties on the material properties of polymer nanocomposites with the new thermoplastic matrix Phe as a matrix material.

EXPERIMENTAL

Chemicals and instrumentation

Phe was supplied by Union Carbide Corp. Mumbai, India. Its glass-transition temperature was 100°C, and its polydispersity index [weight-average molecular weight/number-average molecular weight (M_w/M_n)], determined by gel permeation chromatography, was 1.53 (M_n = 40000 g/mol, M_w = 62,000 g/mol). Tetrahydrofuran was used as a solvent throughout the study. Red mud was provided by R&D Laboratory of NALCO (Damanjodi, Orissa, India). Phosphomolybdic acid was obtained from LOBA Chemie Pvt., Ltd. (Mumbai, India). Aniline and formaldehyde was obtained from Merck, Ltd. (Mumbai, India).

Attenuated total reflection spectra in the range 4000–400 cm^{-1} of the polymer nanocomposite films were measured with Fourier transform infrared (FTIR) spectroscopy (Nexus 8700, Thermo Nicolet, Madison) and Omnic software, and a uniform resolution of 2 cm^{-1} was maintained in all cases.

The nature of the polymer nanocomposite films was investigated by means of X-ray diffraction (XRD; PW 1710 diffractometer unit, Philips, Almelo, The Netherlands) with Cu Kα radiation generated at 40 kV and 20 mA at a scan rate of 0.5°/min; the diffraction angle (2θ) range was 2–10° for red mud and modified red mud, whereas the range for the pure polymer and polymer nanocomposite materials was 5–70°.

Field emission scanning electron microscopy (FESEM; JSM 5800, JEOL, Tokyo, Japan) was used to analyze the morphological images of the raw red mud and modified red mud.

Transmission electron microscopy (TEM) was used to characterize the size of the particles present in the nanocomposite systems. TEM analysis was done by a JEOL instrument (JEN-2100).

Thermal analysis was carried out with a Perkin Elmer Instrument Pyris Diamond dynamic thermal analysis/thermogravimetry apparatus, Norwalk under the atmosphere at a heating rate of 10°C/min.

Preparation of phosphomolybdic acid modified red mud (PRM)

A known amount of raw red mud was first washed with distilled water two to three times and then dried in an oven. When the red mud was completely dried; it was treated with a 5*M* solution of phosphomolybdic acid for 24 h. Then, it was filtered, dried, weighed, and ground to obtain its powdered form. The weight of the red mud increased by 20%. The powder was then sieved through 53-μm mesh to remove the larger particles. The powder thus obtained was fine and acidically modified. Thus, layered silicates and double-layered hydroxides [$Al_2(OH)_7$ and $MgAl(OH)_5$] of red mud were modified with inorganic acids. The inorganic acid modifier compatibilized the silicate and hydroxide surface of the polymer matrices and spaced the crystalline layers apart to minimize the energy needed for the exfoliation process.

Organic modification of red mud

The organic modification of red mud was done by the following two steps:

1. Freshly prepared aniline hydrochloride was mixed with red mud with a magnetic stirrer.
2. Formaldehyde was then added drop by drop to the mixture with intense stirring action.

The addition of aniline hydrochloride to red mud replaced the cation present in the octahedral sites of the silicate with aniline occupying the same. The formaldehyde added formed a condensation oligomer as the product with the pendent group as

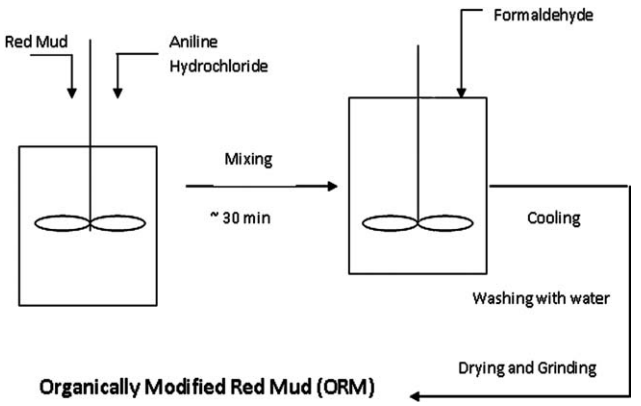

Figure 1 Experimental setup for the organic modification of red mud.

formaldehyde that was compatible with the polymer. The ratio of aniline to formaldehyde was kept at 1 : 1 to stop any further condensation of the aniline and formaldehyde, as this could have led to a polymer blend-type nanocomposite, which could have the problems associated with the miscibility of polymer blends, and this filler would not have been a universal filler for the polymer matrix. Figure 1 depicts the experimental setup for the organic modification of red mud.

Mechanism

Figure 2 shows the mechanism and condensation reaction between substituted aniline and formaldehyde. After the substitution of the metal cation, the condensation reaction occurred between the substituted amine group with extra hydrogen and the formaldehyde molecule to form water as a byproduct. Thus, the organic entity entered the space between the silicate layers; this provided a suitable site for binding the polymer. When this filler was mixed with the polymer, the polymer chains were attracted by the presence of the organic species at the interlayer spaces and, thus, got intercalated between the layers, which had about nanometer-size openings.

Preparation of poly(hydroxy ether) of bisphenol A/phosphomolybdic acid modified red mud nanocomposite (PRC) materials and poly(hydroxy ether) of bisphenol A/organically modified red mud nanocomposite (PNC) materials

A 10% (w/v) solution of Phe was prepared by the dissolution of dried Phe in tetrahydrofuran with continuous stirring at 50°C. The polymer nanocomposite films were made by the mixture of different loading percentages of PRM and organically modified red mud (ORM) into the virgin Phe solution; the mixture was stirred constantly and sonicated for 0.5 h for better dispersion. The compositions of the polymer nanocomposite materials were varied from 0 to 3 wt % modified red mud with respect to the Phe content. The samples were designated as shown in Table I.

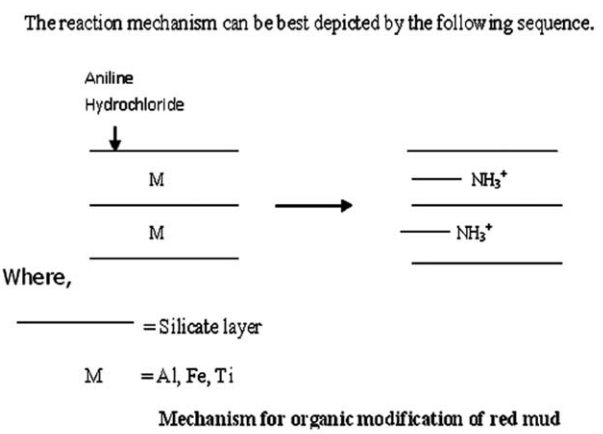

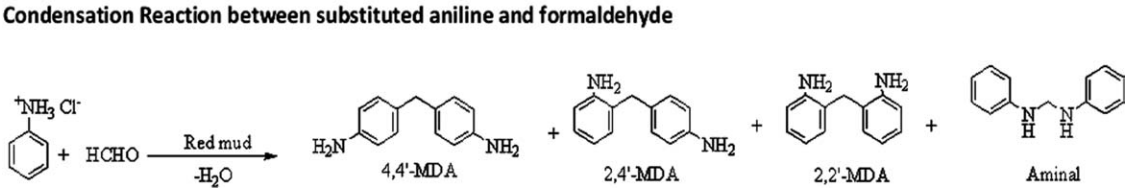

Figure 2 Mechanism and condensation reaction for the organic modification of red mud. MDA, meta diamine.

TABLE I
Sample Designation

Sample	Filler loading (%)
Phe	0
PRC1	1.0
PRC2	2.0
PRC3	3.0
PNC1	1.0
PNC2	2.0
PNC3	3.0

RESULTS AND DISCUSSION

FTIR spectroscopy

The FTIR spectra in Figure 2 show the presence of characteristic peaks of Phe. The characteristic vibration band of Phe for hydroxyl stretching vibrations (O—H) having polymeric associations was observed at 3394 cm^{-1}, whereas the alkyl stretching band of C—H was observed at 2974 cm^{-1}, and the aryl stretching band of C—H appeared at 3037 cm^{-1}. The peak at $\nu = 1183$ cm^{-1} was due to C—O stretching of the phenyl ether linkage. Furthermore, the peak at $\nu = 1607$ cm^{-1} was attributed to the aromatic ring.

Figure 2 also shows the spectra of Phe/modified red mud nanocomposite membranes with different loading percentages of the filler. The characteristic vibration band of PRC3 for hydroxyl stretching vibrations (O—H) was observed at 3270 cm^{-1}. The intensity of the O—H stretching vibration peak decreased, and the peak frequency shifted from 3394 to 3270 cm^{-1}, that is, to a lower frequency compared to that of pure phenoxy. The redshift in the hydroxyl stretching frequency occurred because of the various degrees of hydrogen bonding between the polymer and the filler; this lengthened and weakened the O—H bond and, hence, lowered the vibrational frequency. The alkyl stretching band of C—H in case of PRC3 also showed a redshift from 2974 to 2861 cm^{-1} because of the interaction of modified red mud with the polymer matrix. Similarly, the peak at $\nu = 3036$ cm^{-1} was attributed to the stretching vibrations of the aryl C—H band, at a slightly lower frequency than that of the pure phenoxy. The other characteristic vibrational frequencies of PRC3 are presented in Table II.

The spectra of PNC2 and PNC3, as shown in Figure 3, showed the disappearance of the hydroxyl stretching frequency (O—H). The disappearance of the hydroxyl peak depicted complete physical interaction of the O—H group with different groups of the ORM; this, thereby, did not leave any free hydroxyl groups. However, the alkyl stretching bands of C—H for PNC2 and PNC3 were observed at 2948 and 2947 cm^{-1}, respectively. The redshift in the alkyl stretching frequency C—H of PNC2 and PNC3 as compared to the pure phenoxy showed interaction of the filler with the polymer matrix.

TABLE II
Assignment of FTIR Spectral Bands for Pure Phenoxy, PRC, and PNC Membranes

Group	Phe (cm^{-1})	PRC3 (cm^{-1})	PNC2 (cm^{-1})	PNC3 (cm^{-1})
OH	3394	3270	—	—
C—H	2974	2861	2948	2947
C—H (Ar)	3037	3036	3016	3020
NH_3+	—	—	1571	1572
C—O	1183	1168	1182	1180
C=O	—	1766	1760	1760
Ar	1607	1613	1499	1503
Si—O	—	953	952	951
Mo—O_c—Mo	—	896	—	—

The characteristic vibrational frequencies of PNC2 and PNC3 at $\nu = 1571$ and 1572 cm^{-1}, respectively, was attributed to the stretching frequency of ammonium ions (NH_3^+'s); this depicted the formation of zwitterions. The other vibrational frequencies associated with PNC2 and PNC3 are tabulated in Table II. ORM showed better interaction with the Phe matrix than PRM; therefore, we inferred that ORM would show better dispersion in the polymer matrix than PRM.

XRD study

Wide-angle XRD studies were performed on raw red mud and the modified red mud, as shown in Figure 4.

The spacing of the (001) basal reflections of the raw red mud and PRM was measured and is shown in Table III. The basal spacing of the PRM was larger than that of the raw red mud.

In the ORM, the case appeared to be slightly different, with the peak being lost. Thus, we inferred that the silicate layers underwent exfoliation or

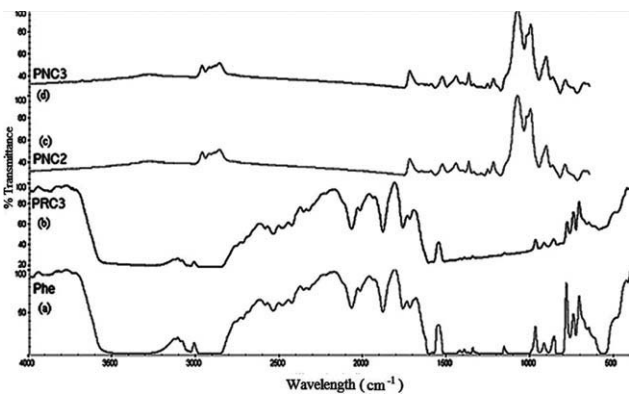

Figure 3 FTIR spectra of (a) pure Phe, (b) PRC3, (c) PNC2, and (d) PNC3.

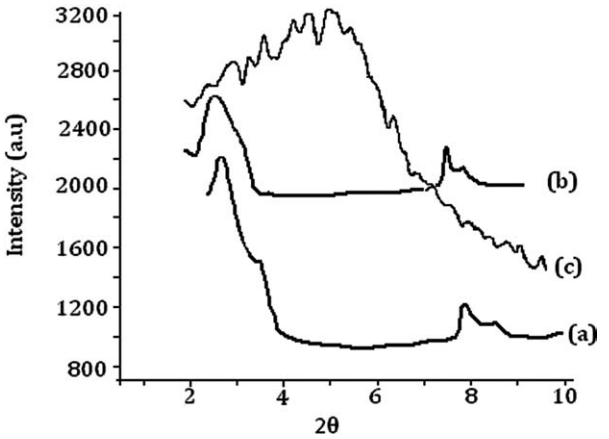

Figure 4 XRD patterns of (a) raw red mud, (b) PRM, and (c) ORM.

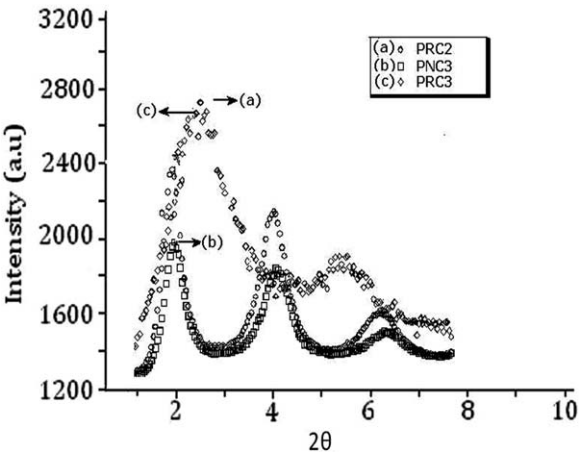

Figure 5 XRD patterns of (a) PRC2, (b) PNC3, and (c) PRC3.

random dispersion in the modification stage itself. This suggested that the aniline formaldehyde type precursor formed a coating on the partially exfoliated silicate layers; this led to random dispersion and rendered the absence of peaks in the XRD micrograph.[27]

The wide-angle diffraction patterns of the PRC2 and PRC3 films are shown in Figure 5. The crystallinity of the composite membranes was mainly due to Phe. The characteristic diffraction peaks for PRC2 and PRC3 were observed at 2θ values of 2.36 and 2.26°. The diffraction peak at $2\theta = 2.26°$ was considerably broadened, and the interplanner distance also widened compared to the raw red mud and PRC2 nanocomposite; this indicated intercalation of the phenoxy matrix within the nanofiller of the nanocomposite membranes.

The polymer nanocomposite films showed a decrease in the intensity of the crystalline peak as the loading percentage of ORM increased. The decrease in the intensity of the crystalline peaks showed an increase in the disorderliness of the interlayers of modified red mud.

As shown in Table IV, it was clear that the basal spacing for PRC3 was larger than those of the other PRM-based nanocomposites materials; this provided evidence for the better intercalation of the polymer matrix within the silicate galleries of the filler in the case of the PRC3 compared to the rest of the nanocomposites.

The XRD pattern of the phenoxy/ORM nanocomposite membranes are shown in Figure 5.The characteristic diffraction band of PNC3 was observed at $2\theta = 2.11°$. The increase in the interlayer distance of the silicate galleries of ORM indicated that Phe was successfully intercalated into the silicate layers.

FESEM

FESEM has evolved, and the electron beam cross section has become smaller and smaller, which has increased the magnification several fold. Raw red mud and modified red mud were characterized by FESEM, as shown in Figure 6. The FESEM analysis showed that the raw red mud consisted of aggregates, including particles of different dimensions. The FESEM images of PRM and ORM showed a very fine distribution of particles with sizes of 64 and 71 nm, respectively, as shown in Figure 7. Although ORM showed a more homogeneous distribution of particles than raw red mud with particle sizes larger than PRM due to the formation of an organic coating around the particles.

TEM

TEM complements XRD by showing a very small section of the material for the possibility of intercalation or exfoliation. It also provides information about the particle size and nanodispersion of particles. It, however, supplies information on a very local scale. However, it is a valuable tool because it

TABLE III
XRD Basal Spacing Results for the Raw Red Mud and PRM

Sample	2θ	*d*-Spacing (Å)
Raw red mud	2.71	32.76
PRM	2.46	36.72

TABLE IV
XRD Results for the PRC and PNC Membranes

Sample	2θ	*d*-Spacing (Å)
PRC2	2.36	37.56
PRC3	2.26	39.48
PNC3	2.11	41.62

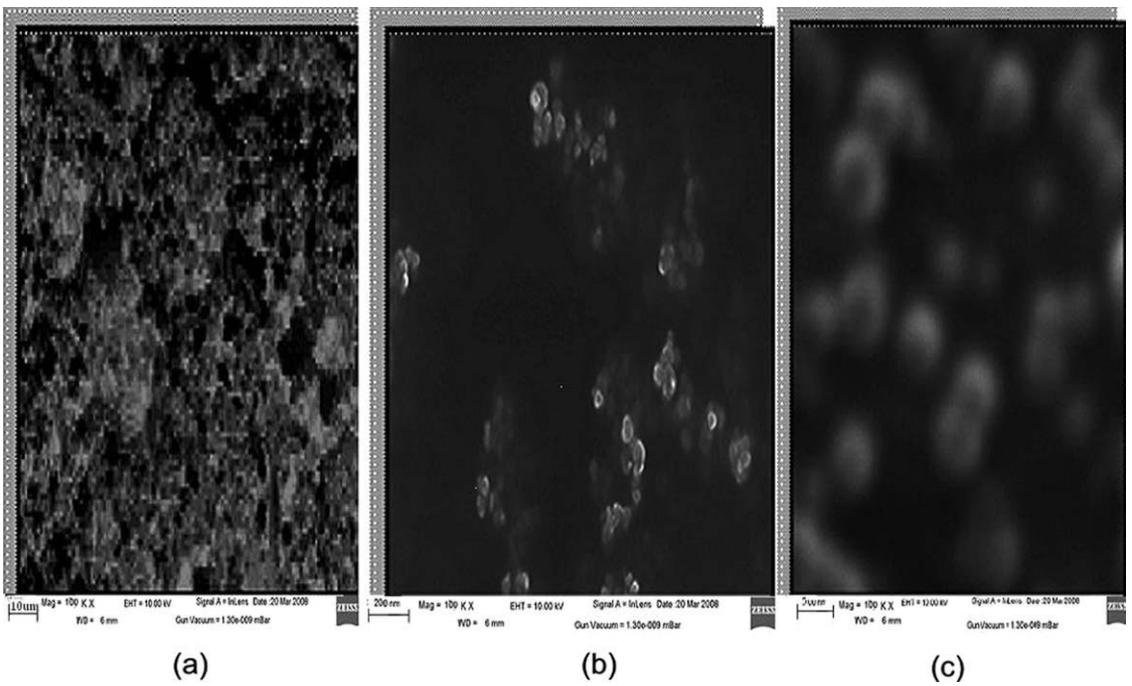

Figure 6 FESEM images of (a) raw red mud, (b) PRM, and (c) ORM.

enables one to see the polymer and filler on a nanometer scale.

Figure 8(a) shows a representative TEM image of the PNC3 with a 3 wt % loading percentage of ORM in the phenoxy matrix, whereas Figure 8(b) shows a representative TEM image of PRC3. As shown in Figure 8(a), a rather good dispersion of ORM was achieved. It was clear that the area covered by the red mud, shown in Fig. 8(a), was larger than that shown in Figure 8(b); this indicated a more extended platelet separation and the overall best nanodispersion of the critical loading at 3 wt % ORM in the phenoxy matrix.

The average particle size was found to be 14 nm for PNC3, as shown in Figure 8(a), whereas the average size of the particles in PRC3 was found to be 19 nm, as shown in Figure 8(b).

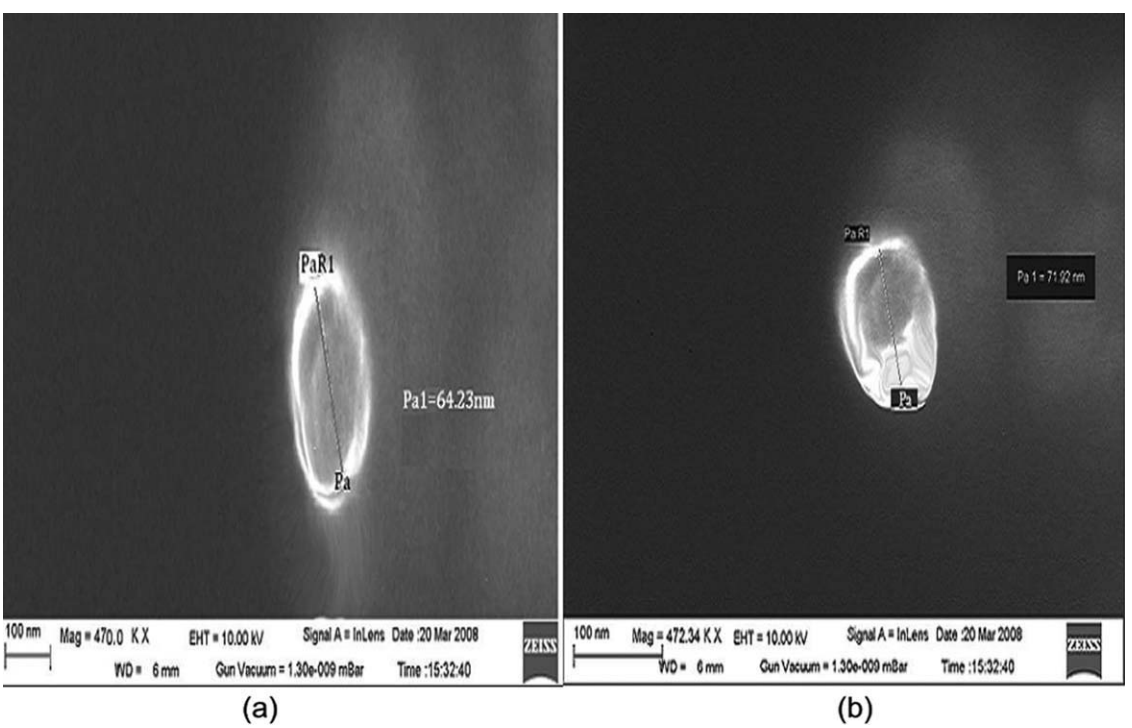

Figure 7 FESEM images depicting the size of a single red mud particle for (a) PRM and (b) ORM.

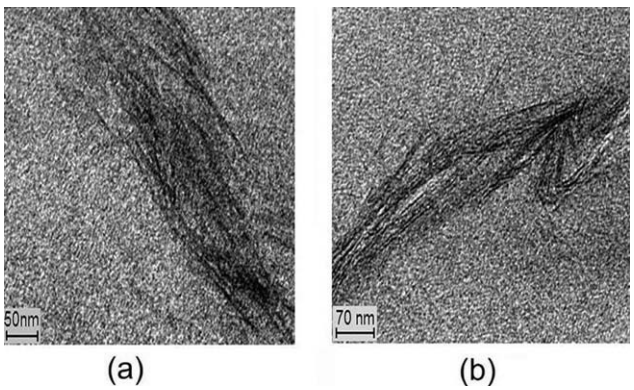

Figure 8 TEM micrographs of (a) PNC3 and (b) PRC3.

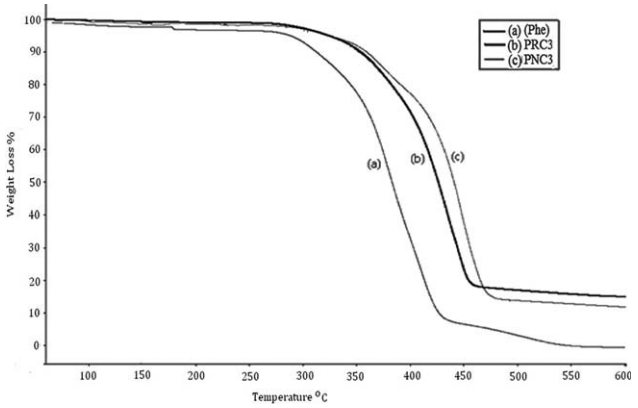

Figure 9 Typical TGA thermograms of (a) Phe, (b) PRC3, and (c) PNC3.

As shown in Figure 8(b), the nanoparticles showed a certain extent of agglomeration and the formation of interconnected aggregates or tactoids of silicates.

There may have been several fundamental problems that affected the polymer–particle interactions in solution and that resulted in disordered nanoparticle aggregates. These problems may have arisen from competing interactions among the solvent, polymer chains, and filler particles. The conformation of the polymer chains adhered to the nanoparticles also influenced the ordered dispersion of the particles.

The presence of ORM and PRM with different loading percentages and dispersion capabilities may help us to identify the main structural driving force for dispersion in these Phe-based polymer nanocomposites. It has been reported that the interaction between the polymer chains and the inorganic surface of clay[28] is crucial in polar polymers, and therefore, it could also have existed between the polar Phe and the modified red mud surface. A good dispersion of modified red mud in the polymer matrix had a significant effect on the properties of the nanocomposites.

Thermogravimetric properties

The thermal stability of the pure Phe and Phe nanocomposite membranes with different filler contents was investigated by thermogravimetric analysis (TGA). The TGA thermograms corresponding to the thermal decomposition of the pure phenoxy and Phe nanocomposite films are shown in Figures 9 and 10. As shown, both the pure polymer and nanocomposite materials decomposed in a single stage. When we compared the thermal stability of the polymer and the critical loading percentage of the nanocomposite membranes of PNC3 and PRC3, it was clear that PNC3 was more stable than the pure phenoxy and PRC3. The pristine Phe was thermally stable up to 275°C. Because the Phe nanocomposite membranes showed enhanced thermal stability, the initial decomposition temperature (T_i) of the phenoxy occurred at 276°C, whereas in PNC3 and PRC3, the T_i values were found to be 318 and 298°C, respectively, as shown in Table V. Similarly, the final decomposition temperatures (T_f's) of phenoxy, PNC3, and PRC3 were observed at 433, 479, and 458°C, respectively. The enhancement in the thermal stability of PNC3 was attributed to the better compatibility and intercalation of polymer matrix within the silicate galleries of 3 wt % ORM. Similarly, as shown in Figure 10 and Table V, PNC2 showed higher T_i and T_f values compared to PRC1 and PRC2, thereby showing a higher thermal stability comparatively. In general, major weight losses were observed in the range 275–500°C for Phe and the polymer nanocomposite films; this range may have corresponded to the structural decomposition of the polymer backbones at higher temperatures. After 500°C, all of the curves became flat, and mainly, the inorganic residue (i.e., Al_2O_3, MgO, and SiO_2) remained.

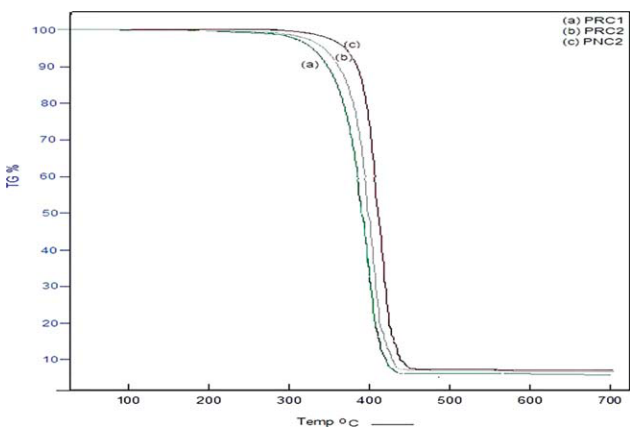

Figure 10 TGA thermograms of (a) PRC1, (b) PRC2, and (c) PNC2. [Color figure can be viewed in the online issue, which is available at wileyonlinelibrary.com.]

TABLE V
Degradation Temperatures and Ash Contents of the Pristine Phe, PRC, and PNC Membranes

Sample	T_i (°C)	T_f (°C)	Ash (%)
Pure Phe	276	433	3.2
PRC1	287	439	6.33
PRC2	293	443	7.97
PNC2	312	454	8.23
PNC3	318	479	11.30
PRC3	298	458	14.15

CONCLUSIONS

FTIR spectroscopy showed a redshift in the absorption peaks of the hydroxyl groups of the nanocomposite materials with increasing loading percentage of the filler content in the polymer matrix. This was attributed to its pendent hydroxyl group, which was very prone to chemical interactions with the polar groups of the filler. The addition of ORM also showed a redshift in the characteristic peaks of the nanocomposite materials upon intermolecular hydrogen-bond formation; this suggested that interaction occurred between the polymer matrix and the modified filler. The FESEM analysis of PRM showed a particle size of 64 nm, whereas ORM showed a particle size of 71 nm. In the Phe-based nanocomposites, mostly intercalated structures were produced in the acid-modified red mud modifications, but modification by organic moieties (ORM) resulted in a mixed intercalated–exfoliated structure. TEM images of the Phe nanocomposite membranes showed homogeneous nanophase dispersion of the modified filler in the Phe matrices with an average particle size of 14 nm in the case of PNC3, whereas an average particle size of 19 nm was revealed for PRC3. The thermal stability of the polymer also increased after nanocomposite preparation because the red mud acted as a heat barrier; this enhanced the overall thermal stability of the system and assisted in the formation of char after thermal decomposition.

References

1. Huang, H. H.; Orler, B.; Wilkes, G. L. Macromolecules 1987, 20, 1322.
2. Surivet, F.; Lam, T. M.; Pascault, J. P.; Pham, Q. T. Macromolecules 1992, 25, 4309.
3. Novak, B. M.; Ellsworth, M. W. Mater Sci Eng A 1993, 162, 257.
4. Hajji, P.; David, L.; Gerard, J. F.; Pascault, J. P.; Vigier, G. J Polym Sci Part B: Polym Phys 1999, 37, 3172.
5. Shao, C.; Kim, H.-Y.; Gong, J.; Ding, B.; Lee, D.-R.; Park, S.-J. Mater Lett 2003, 57, 1579.
6. Gupta, V. K.; Sharma, S. J. Environ Sci Technol 2002, 36, 3612.
7. Thakur, R. S.; Das, S. N. In Red Mud—Analysis and Utilization; Sivakamasundari, S., Ed.; Wiley: New Delhi, 1994.
8. Ayres, R. U.; John, H.; Bjorn, A. MRSI Bull 2001, 7, 477.
9. Tsakiridis, P. E.; Agatzini-Leonardou, S.; Ustadakis, P. O. J Hazard Mater 2004, 116, 103.
10. Mymrin, V.; de Araujo Ponte, H.; Lopes, F. O.; Vaamonde, V. A. Green Chem 2003, 5, 357.
11. Amritphale, S. S.; Patel, M. Silicates Ind 1987, 2, 31.
12. Vincenzo, M. S.; Renz, C.; Stefano, M.; Giovanni, C. J Eur Ceram Soc 2000, 20, 245.
13. Yalcin, N.; Sevnic, V. Ceram Int 2000, 26, 485.
14. Asokan, P.; Saxean, M.; Asolekar, S. R. Resour Conserv Recycl 2005, 43, 239.
15. Singh, M.; Upadhayay, S. N.; Prasad, P. M. Cem Concr Res 1997, 27, 1037.
16. Vincenzo, M. S.; Renzo, C.; Stefano, M.; Giovanni, J. C. J Eur Ceram Soc 2000, 20, 235.
17. Ordonez, S.; Sastre, H.; Diez, F. V. J Hazard Mater 2001, 81, 103.
18. Browner, R. E. Hydrometallurgy 1995, 37, 339.
19. Wagh, A. S.; Douse, V. E. J Mater Res Soc 1991, 6, 1094.
20. Tauber, T.; Hill, R. K.; Crook, D. N.; Murray, M. J. J Aust Ceram Soc 1971, 7, 12.
21. Knoght, J. C.; Wagh, A. S.; Reid, W. A. J Mater Sci 1986, 21, 2179.
22. Gurmendi, U.; Eguiazabal, J. I.; Nazabal, J. Compos Sci Technol 2006, 66, 1221.
23. Bhat, A. H.; Banthia, A. K. J Appl Polym Sci 2007, 103, 238.
24. Bhat, A. H.; Banthia, A. K. Adv Mater Res 2007, 29, 333.
25. Chand, N.; Hashmi, S. A. R. J Sci Ind Res 1999, 58, 795.
26. Chand, N.; Hashmi, S. A. R. Bull Mater Sci 1999, 22, 801.
27. Alexandre, M.; Dubois, P. Mater Sci Eng R 2000, 28, 1.
28. Fornes, T. D.; Hunter, D. L.; Paul, D. R. Macromolecules 2004, 37, 1793.